Preprints.org

Article

Variable Blade Inertia in State-of-the-Art Wind Turbine Structural-Dynamics Models

Laurence Alhrshy [*] , Alexander Lippke , Clemens Jauch

Article

Variable Blade Inertia in State-of-the-Art Wind Turbine Structural-Dynamics Models

Laurence Alhrshy [1,*], Alexander Lippke [2] and Clemens Jauch [1]

[1] Wind Energy Technology Institute, Flensburg University of Applied Sciences, Kanzleistraße 91-93, 24943 Flensburg, Germany; clemens.jauch@hs-flensburg.de

[2] AEROVIDE GmbH, Provianthausstr. 9, 24768 Rendsburg, Germany; Alexander.Lippke@aerovide.com

* Correspondence: laurence.alhrshy@hs-flensburg.de; Tel.: +49-461-48161-407

Abstract: This paper presents a comparison of two methods to represent variable blade inertia in two codes for aero-servo-elastic simulations of wind turbines: the nonlinear aeroelastic multi-body model HAWC2 and the nonlinear geometrically exact beam model BeamDyn for OpenFAST. The main goal is to enable these tools to simulate the dynamic behavior of a wind turbine with variable blade inertia. However, in order to simulate the structural response of wind turbines with variable blade inertias, the source code of load simulation tools need to be modified. This is due to the fact that, currently, state-of-the-art load simulation tools for wind turbines are unable to simulate variable rotor blade inertias. The validity of the modified codes is proven based on a simple beam model. The validation shows very good agreement between the modified codes of HAWC2, BeamDyn and an analytical calculation. The add-on of variable blade inertias is applied to reduce the mechanical loads of a 5 megawatt reference wind turbine with an integrated hydraulic-pneumatic flywheel in its rotor blades.

Keywords: BeamDyn; flywheel; HAWC2; load simulation; OpenFAST; variable blade inertia; wind turbine

1. Introduction

The mechanical properties of wind turbine (WT) rotor blades should not change during their operational life. However, in many cases these properties can be changed, e.g., in smart blades [1], by using a hydraulic-pneumatic flywheel (FW) [2] or structural control (StC) [3], or as a result of atmospheric ice accretion on the blades [4] or rotor imbalance [5]. Such changes in the mechanical properties of rotor blades affect the behavior of WTs significantly. In order to analyze the effect of variable blade mechanical properties on the dynamic behavior of a WT, rotor blades with variable mechanical properties must be first implemented in WT load simulation tools. Since state-of-the-art load simulation tools for WTs are designed to deal with constant mechanical blade properties only, the source code of these tools must be modified in order to allow for variation of mechanical properties during a simulation. How the mechanical properties are changed depends on the case of this variation. The case investigated in this paper is a FW. This is due to the obvious advantages of a FW, which are the numerous functionalities of FWs [6] and, most importantly, the possibility to apply this case exactly to other cases, e.g., atmospheric ice accretion on the blades and rotor imbalance, or with small modifications to the StC and smart blades cases.

The FW used in this paper varies the inertia of the rotor blades by moving a fluid mass between a piston accumulator near the blade root and one or more piston accumulators near the blade tip [7,8]. Consequently, the eigenfrequencies of the rotor blades, the drive train and the tower of the WT can be varied by the FW. Additionally, the FW causes a driving or braking torque, which is independent of the aerodynamic torque. This enables the rotor to be accelerated or decelerated without pitching the rotor blades [2,8,9]. To vary the rotor inertia at any arbitrary operating point of

a WT, the FW comprises electrically-driven pumps, which support the centrifugal forces by moving the fluid from the root to the tip accumulators [2,7,8,10].

Previous investigations of the implementation of variable blade mechanical properties in aero-elastic codes of WTs are limited to passive StC [3,11–15]. The application of StC in the context of WTs refers to the addition of tuned mass dampers (TMDs) to a certain point in the blades, nacelle, tower, or substructure. The main purpose of TMDs is either to enhance damping or to generate forces to control the structural response, e.g., reduce the variability in the platform, pitch and tower top fore-aft displacement. The proposed FW can, in addition to its various StC applications, also support a power system in providing different gird services [6]. Examples of FW's StC applications are damping in-plane vibrations of the blades and tower, mitigating excitations from gravitation and wind shear, balancing rotors, and emergency braking [6]. The main FW's grid services are power system stabilization, the steadying of power infeed, fast frequency response, continuous inertia provision and low voltage ride-through [6]. However, the implementation of the FW in the aero-elastic code of a WT requires simultaneous variation of the inertia of several blade nodes. Moreover, all additional forces that result from the fluid movement along the rotating blades must applied to the correct blade nodes.

The implementation of variable blade inertia in aero-elastic codes of WTs has been developed in the last nine years in the Wind Energy Technology Institute (WETI) at Flensburg University of Applied Sciences, Germany. Initially, a First Eigenmodes simulation model of a WT was developed to enable the design of control algorithms [16]. The model was implemented in Matlab/Simulink and consisted of different subsystems, which described the main components of a WT. Since the goal of this model was to facilitate quick simulations, the description level of the WT components was very simple, e.g., rotor blades and tower consisted of only two mass points. In case of the tower, this leads to only two degrees of freedom (DOFs). The rotor blades were represented with three DOFs. Furthermore, the geometrical and the aerodynamical properties of the blade were simplified in the form of a torque coefficient lookup table. Consequently, an exact response of a WT with variable inertias at several nodes along the blade length could not be provided by this model. To do this, a load simulation tool is required that can describe the structural dynamics of the rotor blades in more detail. One such tool is ElastoDyn, a model developed by the National Wind Technology Centre at the National Renewable Energy Laboratory (NREL), USA which is implemented within the aeroelastic modularization framework FAST [17,18]. ElastoDyn is based on Bernoulli-Euler beam theory and describes the mechanical properties of a rotor blade in greater detail than the First Eigenmodes simulation model. Just like the First Eigenmodes simulation model, ElastoDyn is free, publicly available, and well documented. The source code of ElastoDyn has previously been modified to implement variable blade inertia [19]. Although ElastoDyn uses a simple mathematical theory based on Kane's method [20] to establish equations of motion, the exact solutions of ElastoDyn met the needs of previous research, which also dealt with the hydraulic-pneumatic FW [19]. However, the method used in ElastoDyn to implement the resulting forces from the fluid movement simplifies these forces by applying a total (accumulative) torque at the hub [19]. This simplification does not take the impact of the forces on the blade nodes into consideration, which inhibits several applications of the FW, e.g. damping of in-plane vibrations of blades, and mitigation of excitations from gravitation and wind shear, from being simulated. Furthermore, ElastoDyn only supports beams constructed from isotropic material without mass or elastic offsets, without axial or torsional DOFs and without shear deformation. For these reasons, it was obvious that the method of variable blade inertia had to be implemented in a more complex structural dynamics model of WT rotor blades.

Two advanced structural dynamics models, HAWC2 [21] and BeamDyn [22], were to compare and validate the implementation method of variable blade inertia. Both models utilize finite beam element theory to enable a very complex and advanced modelling methods of non-linear beam structural dynamics of the blade structure. The mechanical properties of several cross-sections of the blade are defined in these models by tabular mass and stiffness matrices, which are used in the numerical solution of the dynamic equations during a given simulation. In addition to the extensive description of the blade mechanical properties, a previous comparison of HAWC2 and BeamDyn,

which had shown that both models are capable of computing accurate solutions for highly nonlinear effects [23].

The method used for the implementation of variable blade inertia and the differences obtained by applying this method in HAWC2 and BeamDyn are presented in detail in the following section. In section 3, the modified HAWC2 and BeamDyn models are shown to be valid for analytical calculations of three benchmarking cases of increasing complexity. An application of variable blade inertia is presented for both models in section 4, where an emergency braking is supported with the hydraulic-pneumatic FW.

2. Implementation of Variable Blade Inertia in HAWC2 and BeamDyn

Although the definition of beam elements in the HAWC2 and BeamDyn models is different, the mathematical description of the implementation of variable blade inertia itself is the same in both models. However, due to the differences in the program structure and the accessibility of the source codes of these models, two distinct implementation methods are required.

It should be noted that in this section the matrix notation is used to denote vectorial or vectorial-like quantities. For example, vectors are denoted by an underline $(\underline{\bullet})$, while a double underline $\left(\underline{\underline{\bullet}} \right)$ denotes a tensor, and an overline $(\overline{\bullet})$ denotes a unit vector. The double underline of a matrix denotes the dimension of this matrix.

2.1. Superordinate Model Calculations

As discussed in the introduction, this study focuses on the variation of blade inertia resulting from a change in the global charge state of the tip accumulator, γ_{tip}, of a hydraulic-pneumatic FW. This control variable indicates whether the tip accumulators of individual blades are empty $(\gamma_{tip} = 0)$, or either partly $(0 < \gamma_{tip} < 1)$ or fully charged with fluid $(\gamma_{tip} = 1)$. Based on this variable, its derivatives and the FW geometry, the variable properties of the FW, such as fluid velocity, mass flow, and Coriolis forces, can be calculated. The equations used in this calculation are presented in sections 2.2.1 and 2.2.2. They are implemented in an identical manner in HAWC2 and BeamDyn.

2.2.1 Local Charge State

The FW in each blade has three main components: root accumulator, pipe, and tip accumulator. Each component consists of one or more elements. The geometrical and the mechanical parameters of these elements are integrated in the beam element's properties, which are defined in the input file of the model initialization. The integration comprises the definition of the start, $\underline{R}_{n1,i}$, and the end, $\underline{R}_{n2,i}$, node positions of every FW element, i, within each FW component, j. The geometrical and the mechanical parameters for the tip accumulator are shown in Figure 1.
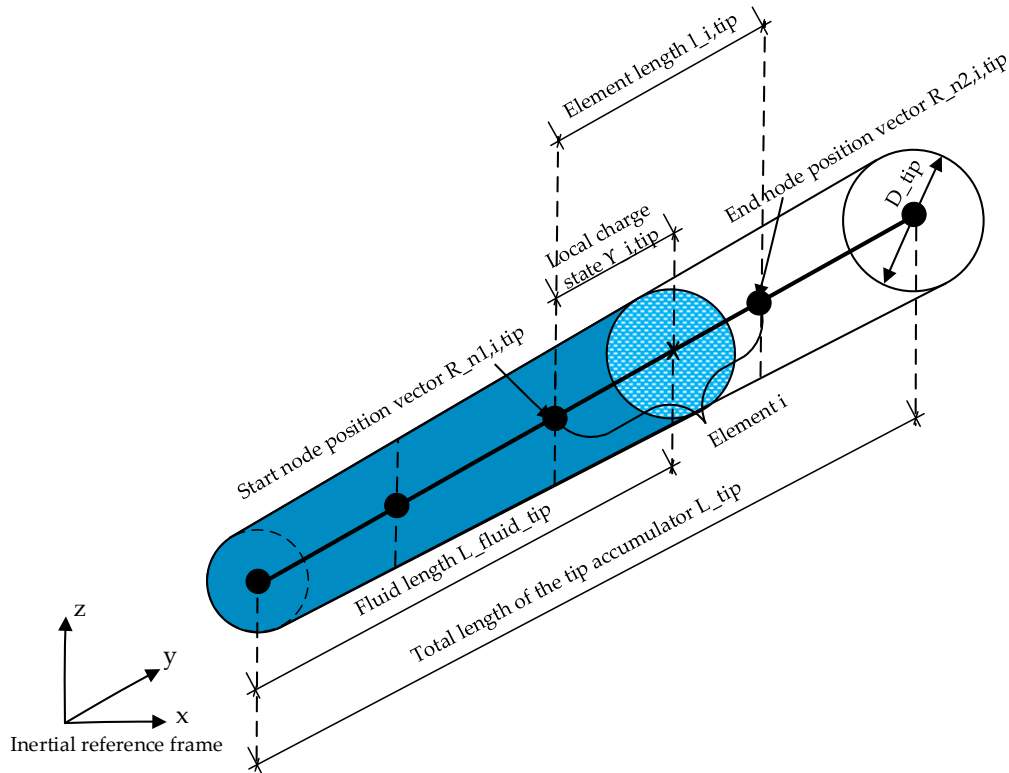
Figure 1. Geometrical input parameters of the tip accumulator.

Using the start, $\underline{R}_{n1,i}$, and end , $\underline{R}_{n2,i}$, positions of the FW elements, the single element lengths, $l_{i,j}$, as well as the total lengths, L_j, of each of the three FW components can be determined using equations (1) and (2).

$$l_{i,j} = \left| \underline{R}_{n1,i,j} - \underline{R}_{n2,i,j} \right| \tag{1}$$

$$L_j = \sum_i l_{i,j} \tag{2}$$

Equation (3) expresses the global charge state of the tip accumulator, γ_{tip}, as the ratio of the volume filled by a fluid, V_{fl}, to the total volume of the tip accumulator, V_{tip}.

$$\gamma_{tip} = \frac{V_{fl}}{V_{tip}} \tag{3}$$

$$V_{tip} = \frac{\pi}{4} \cdot D_{tip}^2 \cdot L_{tip} \tag{4}$$

$$V_{fl} = \frac{\pi}{4} \cdot D_{tip}^2 \cdot L_{fluid\_tip} \tag{5}$$

where V_{tip} and V_{fl} in equations (4) and (5), respectively, are determined from the diameter, D_{tip}, the fluid length, L_{fluid_tip}, and the total length of the tip accumulator, L_{tip}. The global charge state of the root accumulator, γ_{root}, and the local charge state, $\gamma_{i,j}$, in each element of the FW components can subsequently be derived from the global charge state of the tip accumulator, γ_{tip}.

The flow rate in the pipe, root and tip accumulators is constant due to the continuity and incompressibility of the fluid. Thus, the rate of change of the tip charge state, $\dot{\gamma}_{tip}$, can be used in equation (6) to determine the fluid velocities, v_{fl}, in all FW components:

$$v_{fl,i,j} = \frac{V_{tip} \cdot \dot{\gamma}_{tip}}{A_j} \tag{6}$$

Similarly, the fluid acceleration, a_{fl}, can be calculated from from equation (7):

$$a_{fl,i,j} = \frac{\partial v_{fl,i,j}}{\partial t} = \frac{V_{tip} \cdot \ddot{\gamma}_{tip}}{A_j} \tag{7}$$

where A_j is the cross-sectional area of the FW component j, and $\ddot{\gamma}_{tip}$ is the rate of change of $\dot{\gamma}_{tip}$.

2.2.2. Additional Forces Induced by the FW

Three types of forces are induced by the relative motion of the fluid inside the FW components. The forces correspond to the exchange of the angular momentum between the blade stationary structure and the fluid masses. Therefore, the implementation of these forces in HAWC2 and BeamDyn is crucial for a correct representation of the operating FW. The three forces are graphically presented in Figure 2 and are briefly explained below:

1. **Coriolis forces**

The radial movement of the fluid in the FW as the blades rotate produces Coriolis forces. Equation (8) expresses the Coriolis force, $\underline{F}_c$, that is applied to the center of gravitation (COG) of a considered element in terms of cross product, $\times$, the rotational speed of the element, $\underline{\omega}$, with the fluid translational velocity, $\underline{v}_{fl}$, of a fluid mass, m, that is crossing this element.

$$\underline{F}_c = -2 \cdot m \cdot (\underline{\omega} \times \underline{v}_{fl}) \tag{8}$$

2. **Fluid inertial forces**

Acceleration or deceleration of fluid in time causes fluid inertial forces. These forces balance the change of the stored momentum inside the fluid due to the change of the mass flow. Equation (9) expresses the fluid inertial forces in terms of multiplication the fluid mass, m, with the fluid acceleration, $\underline{a}_{fl}$.

$$\underline{F}_{fl,acc} = -m \cdot \underline{a}_{fl} \tag{9}$$

3. **Momentum flux forces**

The change of flow direction or local flow speed of a fluid due to a sudden change in the cross-sectional area causes hydraulic reaction forces to balance the difference in the transported momentum between the inlet and the outlet of a control volume. These forces are called momentum flux forces, $\underline{F}_{fl,mom,i}$, and shown in equation (10) as a difference in the hydraulic reaction forces between two neighbors elements.

$$\underline{F}_{fl,mom,i} = (\dot{m}_{out} \cdot \underline{v}_{fl})_{i-1} - (\dot{m}_{in} \cdot \underline{v}_{fl})_i \tag{10}$$

where $(\dot{m}_{out})_{i-1}$ is the fluid mass flow at the outlet of the previous element, $i-1$, and $(\dot{m}_{in} \cdot \underline{v}_{fl})_i$ is the fluid mass flow at the inlet of the considered element, i.
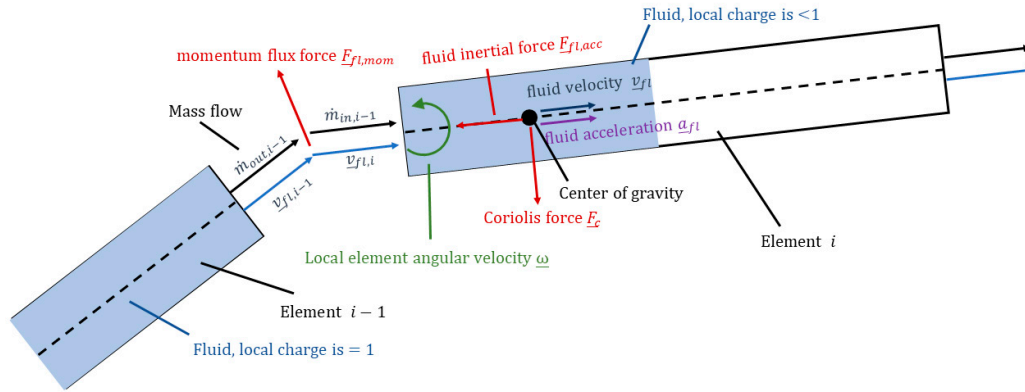
Figure 2. Coriolis force, fluid inertial force, and momentum flux force induced by the FW.

If these three types of forces are treated correctly within the HAWC2 and BeamDyn models, the conservation law of momentum and angular momentum of a WT with a FW in its rotor should still hold. This law is used in section 3 to validate both models.

Other forces, which are related to the stationary effects of the additional fluid masses inside the blade are independent of the translational motion of the fluid. These forces, e.g., gravitational, centrifugal, gyroscopic forces, and inertial forces from fluid without relative motion in any arbitrary direction, are handled inside the original implementation methods in HAWC2 and BeamDyn.

2.3. Implementation of Variable Blade Inertia in HAWC2

HAWC2 is state-of-the-art aeroelastic code developed by the DTU [21], which is used in both academia and industry. The structural dynamics model of HAWC2 is based on the flexible multibody approach using interconnected bodies consisting of Timoshenko finite-element beams. The body motions are described by a method called 'floating frame of reference' [21], described in [24]. The equations of motion (EOM) use a redundant set of coordinates consisting of the body reference motion DOFs, the relative elastic motion DOFs and a set of algebraic constraints [21].

Since HAWC2 is closed source, users cannot create more complex models by changing the source code. For this reason, the HAWC2 developers created a DLL programming interface called the External System interface [25]. This allows the user to define general second-order dynamic equations and general algebraic constraints outside of the HAWC2 core in user-written DLL files. The added external DOFs defined in the DLL files are solved as additional generalized coordinates together with the HAWC2 coordinates in a common equation system [25]. This approach has previously been applied to simulate a planetary gearbox and dynamic mooring lines along with the HAWC2 beam models [25] and was chosen in the present work as the basis to develop a FW model extension with variable inertia.

The general second-order differential-algebraic dynamic equation system of the External System's DOFs and external constraints in a user-written DLL takes the form of equations (11) and (12) [25]:

$$\underline{\underline{M}} \cdot \underline{\ddot{q}} + \underline{\underline{C}} \cdot \underline{\dot{q}} + \underline{\underline{K}} \cdot \underline{q} - \underline{F} + \underline{\underline{G}}_e \cdot \underline{\lambda} = \underline{0} \tag{11}$$

$$\text{and } \underline{g} = \underline{0} \tag{12}$$

where $\underline{\underline{M}}$, $\underline{\underline{C}}$ and $\underline{\underline{K}}$ are the External System's mass, damping and stiffness matrices, respectively. The generalized acceleration, velocity, and coordinates (consisting of the External System's DOFs) are represented by $\underline{\ddot{q}}$, $\underline{\dot{q}}$ and $\underline{q}$, respectively. $\underline{F}$ is the vector of the sum of generalized external forces. .The constraint Jacobian matrix, $\underline{\underline{G}}_e$, and the vector of Lagrange Multipliers, $\underline{\lambda}$, are associated

with the algebraic constraint equations $\underline{g}$. $\underline{G_e}$ and $\underline{\lambda}$ represent constraint reaction forces and thereby transfer loads between the External System and HAWC2 bodies.

The HAWC2 solver solves the set of equations (11) and (12) together with the internal equations of the multibody system with respect to time. This ensures a tight coupling the External Systems' dynamic models with the original multibody system.

2.3.1. Model Idea and Assumptions

The main idea of the FW implementation in HAWC2 is based on that variable inertia can be added via External System, which luse equations (11) and (12) to describe the physical properties.

The overall implementation concept consists of the following ideas and assumptions:

a. By applying fluid dynamics theory using the Eulerian description, the fluid in the FW can be subdivided into several elements forming control volumes (CV), which are fixed relative to the blade beams. Each element is then modeled as an External System.

b. The effects of the contained (static) fluid mass in the CV, which can vary over time, can be addressed by changing the mass matrices $\underline{M}$ and forces $\underline{F}$ associated with the contained mass.

c. The effects associated with the change of the fluid mass (cf. section 2.1) can be added as external forces $\underline{F}$ acting on the CV.

d. To simplify the momentum balance and calculation of mass matrices, a 'lumping' approach was chosen. This means that the flexible pipes and accumulators are approximated as piecewise rigid segments and deformation of a single element as the blade bends is neglected. Thus, each element is of constant size, straight, and cylindrical, implying it can be reduced to a rigid body. Bending of the pipes and accumulators with blade bending is modeled as relative rotation between the rigid elements rather than modelling deformations. This also implies that the stiffness matrix $\underline{K}$ and the damping matrix $\underline{C}$ in equation (11) are 0, and there are no DOFs needed to model deformations.

e. Due to the use of constant-sized cylindrical CVs, stream tube theory can be applied to model the forces from fluid dynamics. Fluid is assumed to change its flow direction only at the connection between two adjacent FW elements. From these assumptions, it follows that equations. (8) to. (10) are sufficient to satisfy the conservation of momentum in the FW.

The implementation concept for the FW is shown schematically in Figure 3 for a simple HAWC2 simulation model with FW elements as External Systems at one blade. This concept uses DLLs developed by AEROVIDE GmbH. The FW can be independently controlled by external control software. The only control signals required during simulation are the global charge state of each blade and their derivatives.
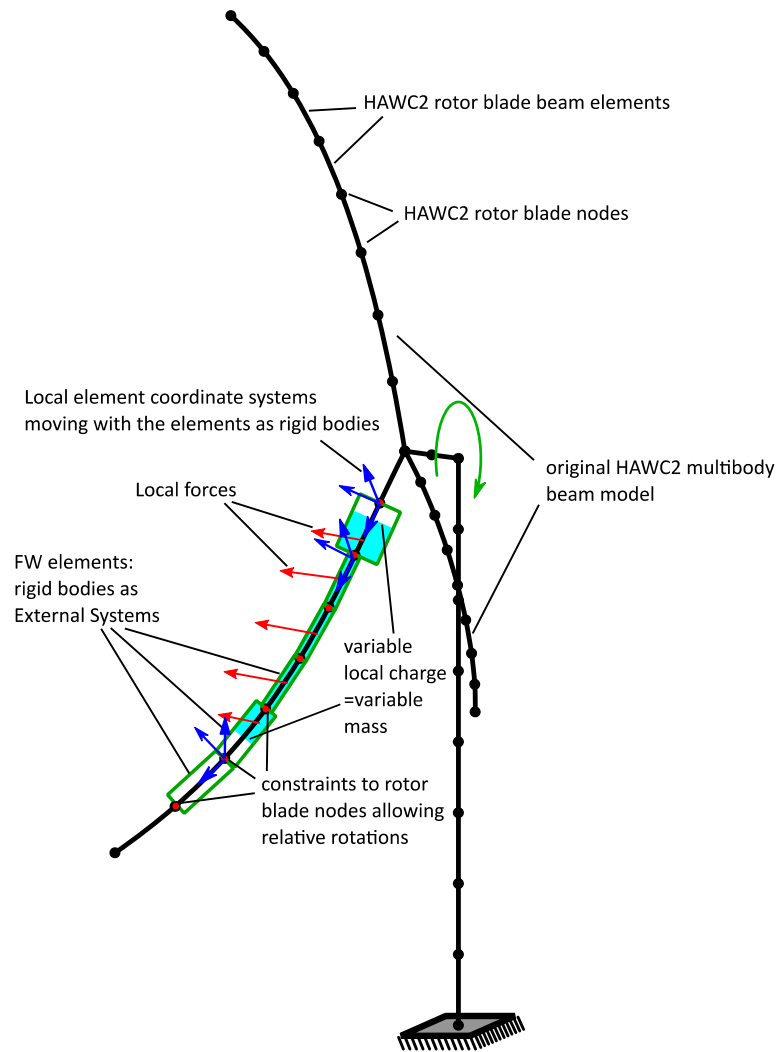
Figure 3. Schematic of a simple HAWC2 simulation model and the additional External System model with FW elements shown at one rotor blade.

2.3.2. Equations of Motion and the Definition of DOFs

As each FW element is assumed to represent a rigid body in 3D space, the Newton-Euler equations are suitable [24] to model their motion and were used in the implementation of the FW model. There are six Newton-Euler equations, (three for translation and three for rotation), which can be seen in equation (13) as a specific form of the general dynamic equations of the External System's DOFs.

$$\underline{\underline{M}} \cdot \begin{pmatrix} \ddot{\underline{R}} \\ \dot{\underline{\omega}} \end{pmatrix} = \begin{pmatrix} \underline{F}_v \\ \underline{M}_v \end{pmatrix} + \begin{pmatrix} \underline{F}_g \\ \underline{M}_g \end{pmatrix} + \begin{pmatrix} \underline{F}_c \\ \underline{M}_c \end{pmatrix} + \begin{pmatrix} \underline{F}_{fl} \\ \underline{0} \end{pmatrix} - \underline{\underline{G}}_e \cdot \underline{\lambda} \tag{13}$$

where $\underline{F}_g$ is the gravitational force. $\underline{F}_c$ is the Coriolis force from equation (8). $\underline{F}_{fl}$ is the sum of the fluid inertial force and the moment force at the element, see equations (9) and (10). $\underline{M}_g$ and $\underline{M}_c$ are the offset moments of the gravitational force and the Coriolis force, respectively, which are caused by the variable COG offset to the element's origin. $\underline{F}_v$ and $\underline{M}_v$ are the centrifugal and gyroscopic force and moment terms, respectively, which occur in the Newton-Euler equations [24].

The Newton-Euler equations are characterized by a specific choice of coordinates for the description of rigid body motion with geometric meanings: The three translational motion DOFs are

described by the element origin's position vector $\underline{R}$ and the acceleration $\underline{\ddot{R}}$, measured in global HAWC2 coordinates. The global HAWC2 coordinates are fixed in space at the ground and thus serve as the inertial reference frame (see HAWC2 manual [21]). The three rotational DOFs are described by the local angular velocity vector $\underline{\omega}$ and the local angular acceleration $\underline{\dot{\omega}}$, measured around the element's own axes. These axes are rigidly fixed to the element and thus always rotate with the element relative to the global HAWC2 coordinates.

As the integrated local rotation coordinates, see equation (14), do not contain unique 3D orientation information of the local element's axes itself [24], the rotations need to be calculated in another way to define the orientation of the local element's axes. To do so, Euler parameters, θ, are used as extra rotation coordinates, as the time derivates of the Euler parameters, $\dot{\theta}$, are related to the local angular velocity vector $\underline{\omega}$ [24]. During each HAWC2 solver update of the 6 External System DOFs ($\underline{R}$, $\underline{\dot{R}}$, $\underline{\ddot{R}}$, $\underline{\varphi}$, $\underline{\omega}$, and $\underline{\ddot{\omega}}$), the associated Euler parameters can be updated by integration, accordingly. The Euler parameters can then be transformed into an element rotation matrix, $\underline{\underline{A}}$, for each time step. The rotation matrix $\underline{\underline{A}}$ finally defines the orientation of the local element's axes with respect to the global HAWC2 coordinate axes [24] (see Figure 3) and is therefore required to transform forces and moments from the local element coordinates to the global HAWC2 coordinates and vice versa.

$$\underline{\varphi} = \int \underline{\omega}\mathrm{d}t \tag{14}$$

The element origin position described by $\underline{R}$ is chosen to be equal to the element's start node position $\underline{R}_{n1,i,j}$. Thus, the origin position and the variable COG position are decoupled. This is a requirement of model assumption (a.), see 2.3.1. The local axes relative to the element are defined with the z-axis pointing from the origin to the element's end node position, $\underline{R}_{n2,i,j}$. Consequently, the z-axis always points in the direction of the element's length axis and the x- and y-axis orientations are arbitrary chosen to be radial to the element, forming a right-handed Cartesian coordinate system (see Figure 4).
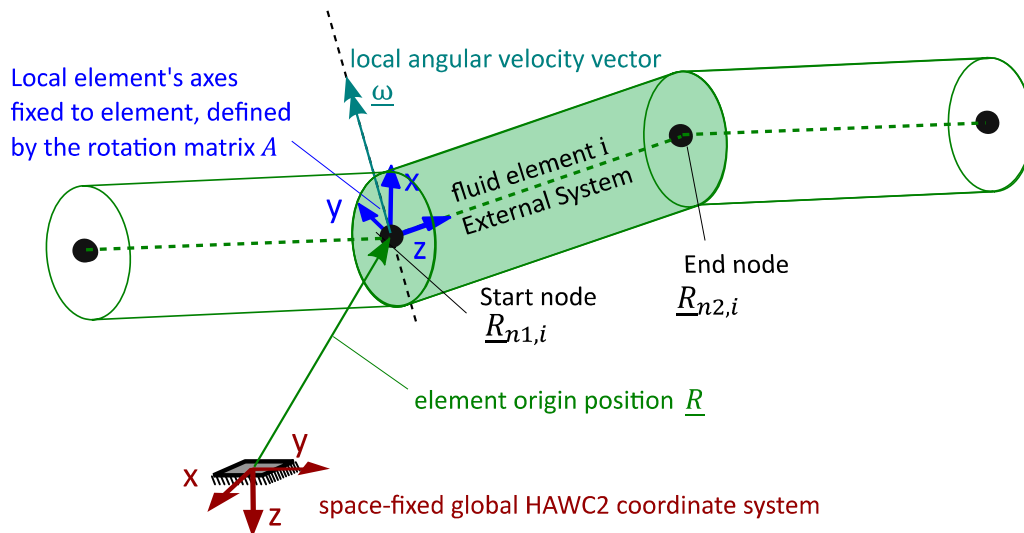

Figure 4. Schematic visualization of a FW element modeled as an external system, showing the global HAWC2 coordinate and the local element coordinate systems, as well as the vectors associated with the motion DOFs of the element.

The mass matrix of a FW element is continuously updated via the superordinate model calculations as the charge state varies. Consequently, the mass matrix in equation (15) takes the form partitioned into translational and rotational DOFs:

$$\underline{\underline{M}} = \begin{pmatrix} \underline{\underline{I_3}} \cdot m & -\underline{\underline{A}} \cdot \underline{\underline{\tilde{u}}}_g \cdot m \\ -\underline{\underline{A}} \cdot \underline{\underline{\tilde{u}}}_g \cdot m & \underline{\underline{J}}_g - m \cdot \underline{\underline{\tilde{u}}}_g \cdot \underline{\underline{\tilde{u}}}_g \end{pmatrix} \tag{15}$$

where $\underline{\underline{I_3}}$ is the 3×3 identity matrix and m is the contained mass. $\underline{u}_g = \begin{pmatrix} 0 \\ 0 \\ z_g \end{pmatrix}$ is the center of

gravity measured in local element coordinates and $\underline{\underline{\tilde{u}}}_g = \begin{pmatrix} 0 & -z_g & 0 \\ z_g & 0 & 0 \\ 0 & 0 & 0 \end{pmatrix}$ is the skew-symmetric

matrix associated with $\underline{u}_g$. Last, $\underline{\underline{J}}_g$ is the inertia tensor measured in local element coordinates referred to the center of gravity.

In the calculation of the mass properties of the elements, they are considered to be solid fluid cylinders with the calculated height of the fluid in the element and the diameter of the element.

2.3.3. Constraints

Without constraints, the Newton-Euler equations would allow the FW elements to move freely in the 3D space. As the FW elements represent additional masses inside the rotor blades, the constraints are formulated such that FW elements are always moving with the rotor blade. The start and end nodes of adjacent elements are always linked like a chain even under blade pre-bending and bending. This can be achieved by constraining both the start and the end nodes of each element, $\underline{R}_{n1,i,j}$ and $\underline{R}_{n2,i,j}$, to nearby nodes of the rotor blade body and allowing rotations of the element relative to the rotor blade nodes. One disadvantage of this approach is that a non-tree-like structure is created because there are constraints at two positions on each element. The non-tree-like structure is commonly called a 'kinematic loop' [26] and causes increased stiffness of the rotor blade when statically overdetermined constraints are used.

So that the kinematic loop does not change blade stiffness or impose numerical problems, the constraint equations of the FW elements are chosen in a manner, that each FW motion DOF is restricted only once. As in applied mechanics, this is achieved in the model by using algebraic constraint equations as a statically-determined simple support for the FW element. Here, the constraints describe a 3-dimensional fixed-floating bearing setup for each FW element. Using the fixed-free bearing setup does not lead to constraint reaction forces at the bearings by bending, axial elongation or torsion between two rotor blade nodes, and thus, there is no influence on the stiffness.

The start and end node positions of the elements, $\underline{R}_{n1,i,j}$ and $\underline{R}_{n2,i,j}$ respectively, can be chosen to coincide with the nodes of the rotor blade body. However, it is also possible to place the FW elements near the rotor blade nodes with a radial offset. This might be desired e.g. to let the FW element's length axis coincide with the blade's mass axis or to follow the real geometric position of the FW component. Both may have an offset to the axis formed by the blade nodes.

The constraint setup and the allowed relative motions are visualized in Figure 5. The required constraint equations can be taken from multibody simulation and robotics textbooks (e.g., [24]).

The fixed bearing restricts relative translational motion between the FW element's start node and a rotor blade node, and additionally rotation around the length axis. Whereas, the floating bearing only restricts relative translational motion between the FW element's end node and a rotor blade node which is radial to the element's length axis.
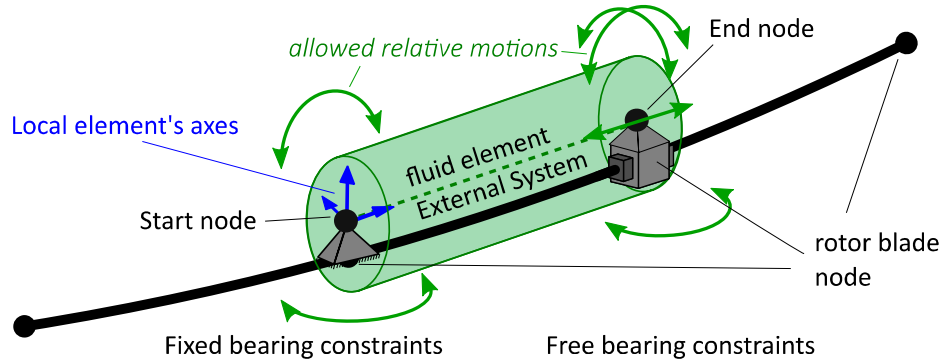
Figure 5. Constraint setup of one exemplary FW element constraint to a rotor blade in the HAWC2 implementation.

2.4. Implementation of Variable Beam Inertia in BeamDyn

BeamDyn is a nonlinear beam finite element model for simulating slender structures, created by the National Wind Technology Center at the National Renewable Energy Laboratory (NREL), USA [22]. The model is used by the FAST aero-hydro-servo-elastic WT multi-physics engineering tool to model blade structural dynamics. BeamDyn uses geometrically exact beam theory (GEBT) [27]. A spatial discretization for the GEBT beam equations is accomplished with Legendre spectral finite elements (LSFEs) [28]. The combination of GEBT and LSFEs enables BeamDyn to model long, flexible, composite WT blades with a single high-order element [22].

BeamDyn is open-source software, which can be used to model the FW directly in its source code. The modelling concept is based on a variable change of the cross-sectional mass matrices during a given simulation and an addition of the forces induced by the FW to the external distributed forces, e.g. aerodynamic forces, hydrodynamic forces, and user defined loads in the BeamDyn input file.

2.4.1. Modification of the Mass Matrix

A blade input file defines the mechanical parameters of the blade in the form of cross-sectional mass and stiffness matrices at various stations along a blade, and six damping coefficients for the whole blade. These parameters are defined as constants in the initialization source code of BeamDyn. Hence, these parameters, e.g. the mass matrix, $\underline{\underline{\mathcal{M}}}$, in equation (16), do not change their values during a simulation. The source code of BeamDyn is modified so the cross-sectional mass matrix parameters are changed from time-invariant parameters to time-variant variables. This modification takes place at the very beginning of the dynamic solution of BeamDyn to ensure that all forces associated to the presence of the additional fluid masses are updated correctly.

The original, $\underline{\underline{\mathcal{M}}}$, and the modified, $\underline{\underline{\mathcal{M}}}^*$, sectional mass matrices are given by equations (16) and (17), respectively.

$$\underline{\underline{\mathcal{M}}} = \begin{bmatrix} m & 0 & 0 & 0 & 0 & -mY_{cm} \\ 0 & m & 0 & 0 & 0 & mX_{cm} \\ 0 & 0 & m & mY_{cm} & -mX_{cm} & 0 \\ 0 & 0 & mY_{cm} & i_{Edg} & -i_{cp} & 0 \\ 0 & 0 & -mX_{cm} & -i_{cp} & i_{Flp} & 0 \\ -mY_{cm} & mX_{cm} & 0 & 0 & 0 & i_{plr} \end{bmatrix} \tag{16}$$

$$\underline{\underline{\mathcal{M}}}^* = \begin{bmatrix} m+m_{fluid} & 0 & 0 & 0 & 0 & -mY_{cm} \\ 0 & m+m_{fluid} & 0 & 0 & 0 & mX_{cm} \\ 0 & 0 & m+m_{fluid} & mY_{cm} & -mX_{cm} & 0 \\ 0 & 0 & mY_{cm} & i_{Edg}+i_{fluid} & -i_{cp} & 0 \\ 0 & 0 & -mX_{cm} & -i_{cp} & i_{Flp}+i_{fluid} & 0 \\ -mY_{cm} & mX_{cm} & 0 & 0 & 0 & i_{plr}+2\cdot i_{fluid} \end{bmatrix} \tag{17}$$

where m and m_{fluid} are the blade structural and the fluid mass density per unit span, respectively; X_{cm} and Y_{cm} are . The local coordinates of the sectional center of mass are expressed by X_{cm} and Y_{cm}. i_{Edg}, i_{Flp} and i_{Fluid} are the edge, flap and fluid mass moments of inertia per unit span, respectively. i_{cp} is the sectional cross-product of inertia per unit span; and i_{plr} is the polar moment of inertia per unit span.

2.4.2. Additional External Distributed Forces

External applied loads including uniformly distributed, point, and tip-concentrated forces can be defined in the input file of BeamDyn. Through customization of the source code, BeamDyn is capable of handling more complex external force cases, such as those induced by the FW. Hence, the three aforementioned types of forces in section *2.2.2.* (Coriolis forces, fluid inertial forces and momentum flux forces) are defined as distributed forces in the dynamic solution subroutines, where are applied every time step. $\underline{\mathcal{F}_{add}}$, shown in equation (18), is the addition of the x, y, and z components of the distributed Coriolis forces, $\underline{\mathcal{F}_c}$, the distributed fluid inertial forces, $\underline{\mathcal{F}_{fl\_acc}}$, and the momentum flux forces, $\underline{\mathcal{F}_{fl\_mom}}$, in the local coordinates.

$$\underline{\mathcal{F}_{add}} = \underline{\mathcal{F}_c} + \underline{\mathcal{F}_{fl\_acc}} + \underline{\mathcal{F}_{fl\_mom}} \qquad (18)$$

Since, the source code allows for the input of applied distributed loads in the global coordinate system, the additional forces, $\underline{\mathcal{F}_{add}}$, must be transformed to the global coordinate system. This transformation is shown in equation (19).

$$\underline{\mathcal{F}_{add}^G} = \underline{\mathcal{R}} \cdot \underline{\mathcal{F}_{add}} \qquad (19)$$

where $\underline{\mathcal{F}_{add}^G}$ represents the additional forces in the global coordinate system and $\underline{\mathcal{R}}$ is the rotation tensor expressed in terms of Wiener-Milenković parameters [29,30]. The additional forces, $\underline{\mathcal{F}_{add}^G}$ can be added to the applied distributed loads.

FAST_SFunc is used to input the global charge state signals and their derivatives in the source code of BeamDyn. FAST_SFunc is a FAST interface to Simulink, which is implemented as a Level-2 S-Function. The Level-2 S-Function is a Simulink block written in C, and it calls a DLL of FAST routines, which are written in Fortran [31,32]. This interface allows external modules such as the control system and the auxiliary systems of the hydraulic-pneumatic FW to be implemented in Simulink. During a simulation, the FW can, hence, be simulated together with the nonlinear aero-elastic tool OpenFAST [33]. However, in order to pass the FW signals through FAST_SFunc, the source code of the OpenFAST glue code needs to be modified. This is because FAST_SFunc is set up to receive only the control signals from the OpenFAST standard modules, such as generator torque control, nacelle yaw control, pitch control, and high-speed shaft brake.

3. Validation

In this section, three benchmarking cases are discussed. The complexity of the cases increases gradually. The main objective of these cases is to validate the method used in HAWC2 and BeamDyn to implement variable blade inertia. The validation is based on the proof of the physical laws of the equilibrium conditions and the conservation of angular momentum. In all three cases, the physical laws are analytically computed and compared with simulation results from the modified HAWC2 and BeamDyn models.

It needs to be mentioned here that BeamDyn standalone is only set up to define a constant angular rotation of the beam root about its rotation axis. Complex root motions such as those treated in Cases 2 and 3 can only be simulated when BeamDyn is used within the WT simulation tool OpenFAST. However, running BeamDyn within OpenFAST requires specification of some physically

realistic generator rotational inertia, even when the generator model is deactivated. Hence, a generator inertia of 115,926 kg-m^2 is used in the simulation as well as in the analytical calculation.

The HAWC2 models for the benchmarking cases are defined in accordance with the demands from BeamDyn within OpenFAST, hence the same beam parameters and additional generator rotational inertia are used.

Case 1: Fixed Rotational Speed of a Fixed, Supported, Straight and Stiff beam

Case 1 concerns the reaction forces and moments of a fixed supported beam that is subjected at its fixed end to a constant rotational speed around the x axis and axial fluid movement along the z axis.

The beam is straight and discretized in 15 elements. The length of each element is 1 m. Three hydraulic components are integrated into the beam: pipe, root and tip accumulators. Each component has 5 elements. The total fluid mass that is moved between the root and the tip accumulators equals 500 kg. A schematic drawing of the beam in charge states 0 and 1 is shown in Figure 6a,b, respectively.
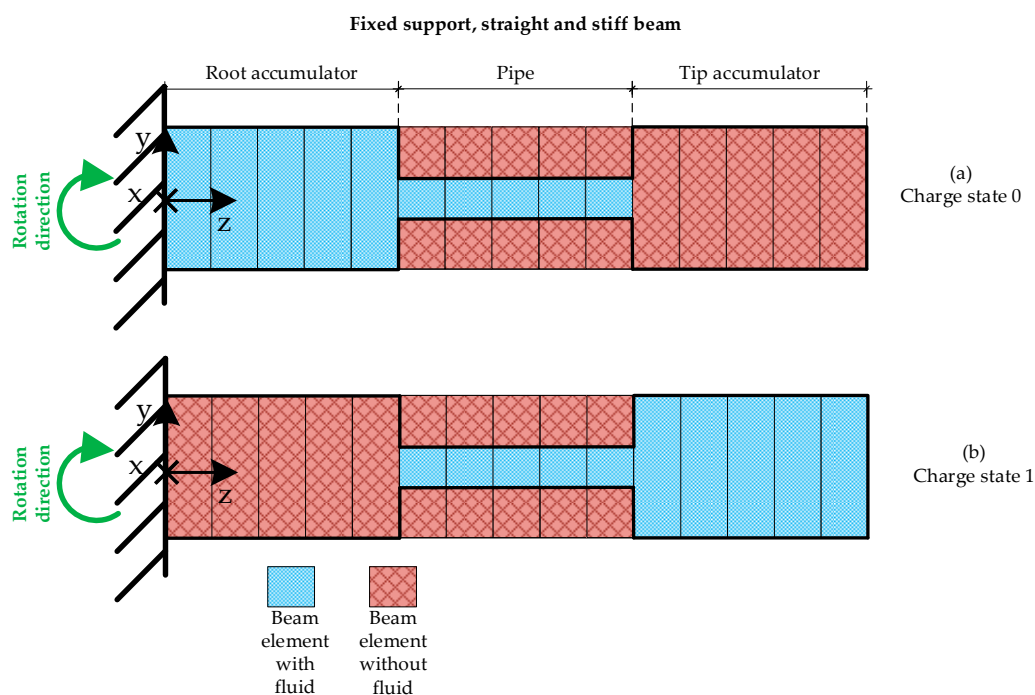
Figure 6. Schematic drawing of the pipe, root and tip accumulators in a fix supported, straight and stiff beam in, (a) a discharged state and (b) a fully charged state.

When the charge state equals 0, the root accumulator is full and the tip accumulator is empty. Conversely, the root accumulator is empty and the tip accumulator is full, when the charge state equals 1. The charge state therefore varies between 0 and 1 as the fluid moves between the root and the tip accumulators.

The input cross-sectional mass and stiffness parameters of the beam are presented in Table 1. In Case 1 and later in Case 2, the beam stiffnesses are set to very high values to prevent the beam from bending. This keeps the local coordinates of the beam elements synchronized with the root coordinates of the beam at the fixed end coordinates of the beam, and simplifies the analytical calculation of the reaction forces and moments.

Table 1. Cross-sectional mechanical properties of the straight and stiff beam.

Beam Element mass Density	Flap and Edge Mass Moments of Inertia per Unit Span	Flap Stiffness	Edge Stiffness	Flap Shear Stiffness	Edge Shear Stiffness	Torsional Stiffness
kg/m	kg·m	N·m²	N·m²	N·m²	N·m²	N·m²
50	50	1.00E+10	1.00E+10	5.00E+08	5.00E+08	1.00E+09

For Case 1, the simulation scenario presented in Figure 7 sets the rotational speed to a constant value of 10 rpm. The charge state rises from 0 to 1 between 10 s and 50 s and remains constant till 60 s. Between 60 s and 100 s the charge state is reduced from 1 to zero and remains at 0 until the end of the simulation. Reaction forces and moments result from the fluid movement. The x, y and z components of these forces and moments are analytically calculated and compared with the corresponding simulation results from HAWC2 and BeamDyn. The comparisons in Figure 7 show a very good agreement between the analytical and the simulated results of all components. The increase/decrease of the y component of the reaction force is due to the Coriolis forces that result from the change in the charge state. Hence, a reaction moment around the x axis results from these Coriolis forces. The z component of the reaction force illustrates the sum of the centrifugal forces and the fluid inertial forces. The variation in the centrifugal forces results from the change in the COG of the beam due to the fluid motion. The fluid inertial forces (Equation (9)) can be seen, when the fluid accelerates, e.g. from 10 to 11 s, or deaccelerates, e.g. from 50 to 51 s.
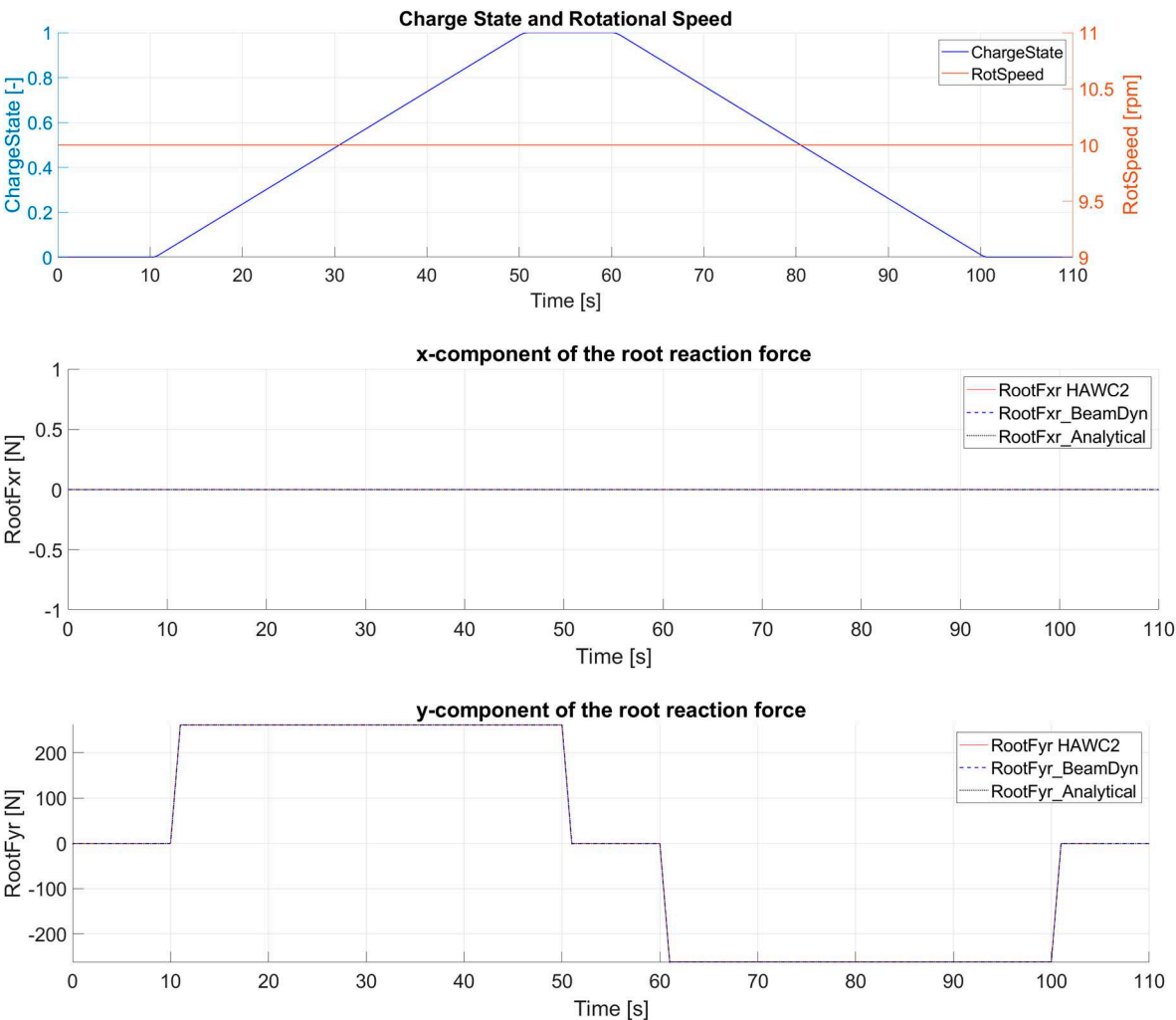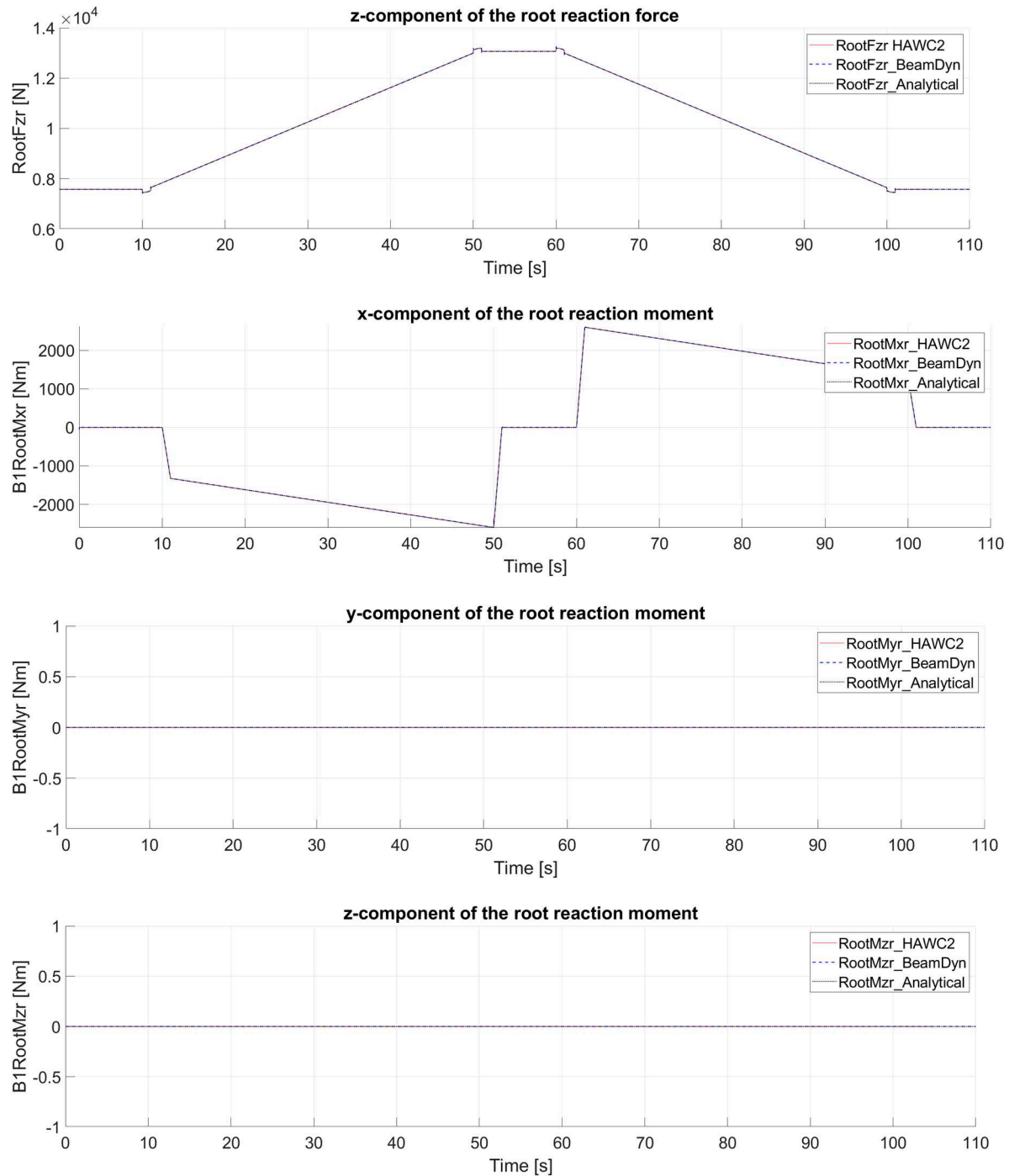
Figure 7. Change in the charge state with a fixed rotational speed. Comparison of the x, y and z components of the analytical reaction forces at the fixed support (dotted black) with the simulated root reaction forces and moments from HAWC2 (red) and BeamDyn (blue dashed).

Case 2: A Pinned-Supported, Straight and Stiff Beam

The purpose of Case 2 is to prove the conservation of angular momentum when the beam inertia changes in a free rotational system. Case 2 uses the same beam that is used in Case 1 but the beam is pinned supported, see Figure 8. This kind of support enables the beam to rotate freely and prevents any translational movement at the supported end. Since the angular momentum in a free rotational system remains constant, the rotational speed of the beam decreases when the beam inertia increases, and vice versa. On this basis, the variable rotational speed of the beam can be analytically calculated. The analytically calculated rotational speed can be used as a reference value to validate the simulated

rotational speed from HAWC2 and BeamDyn. Case 2 uses the same simulation scenario used in Case 1. Figure 9 shows that the increase in charge state leads to an increase in beam inertia, and thus, to a decrease in rotational speed. Conversely, the rotational speed increases when the charge state decreases. The comparison of the analytical calculation with the simulated results in Figure 9b shows a very good agreement.
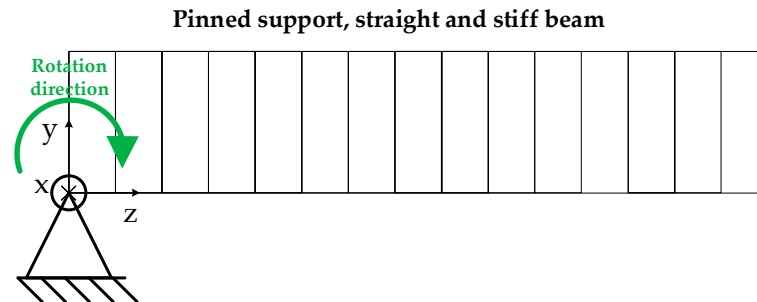

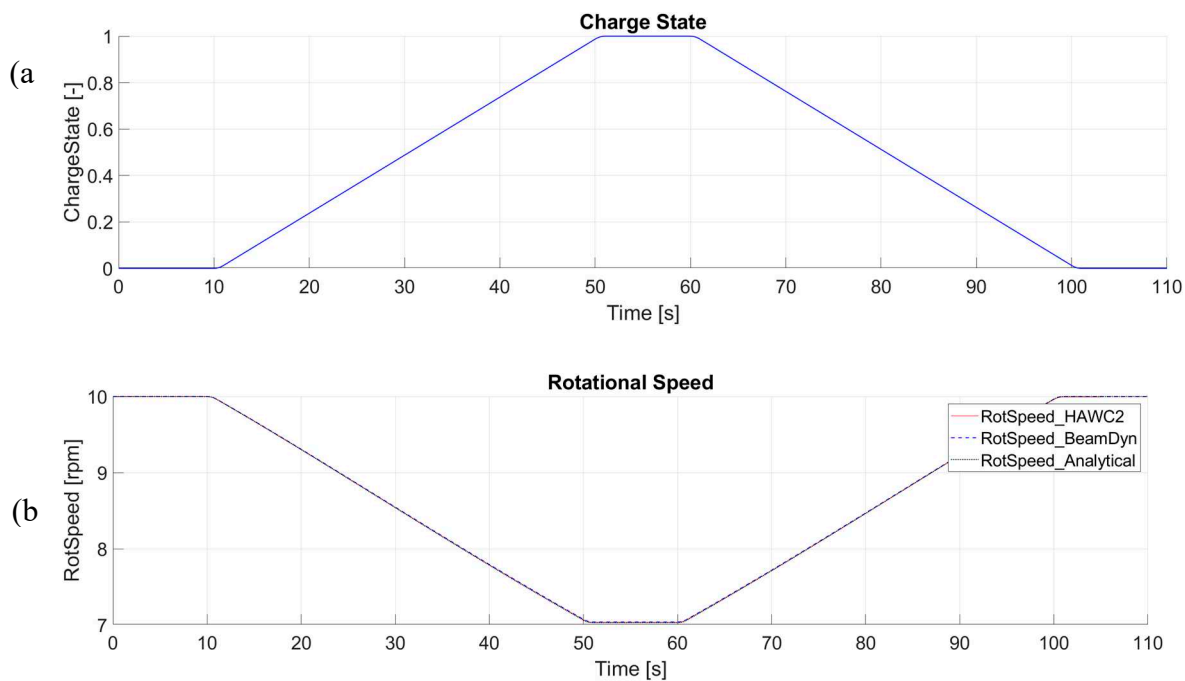**Figure 8.** Schematic drawing of a pinned support, straight and stiff beam.

Figure 9. (a) Change in the charge state; (b) Comparison of the analytical rotational speed (dotted black) with the simulated rotational speed from HAWC2 (red) and BeamDyn (blue dashed) in a pinned-supported, straight and stiff beam.

Case 3: A flexible and Initially Curved Beam

Rotor blades of WTs are manufactured from flexible composite materials using pre-bend or swept designs. Hence, the objective of Case 3 is to compare the ability of the modified HAWC2 and BeamDyn to simulate variable inertia of flexible and initially curved beams. The geometry and the mechanical properties of the beam are shown in Tables 2 and 3.

Table 2. Coordinates of the unloaded beam, showing the pre-bending of the beam.

Section No.	x	y	Z
-	m	m	m
1	0.00E+00	0.00E+00	0.00E+00
2	0.00E+00	1.00E-02	1.00E+00

3	0.00E+00	4.00E-02	2.00E+00
4	0.00E+00	9.00E-02	3.00E+00
5	0.00E+00	1.60E-01	4.00E+00
6	0.00E+00	2.50E-01	5.00E+00
7	0.00E+00	5.63E-01	7.50E+00
8	0.00E+00	1.00E+00	1.00E+01
9	0.00E+00	1.21E+00	1.10E+01
10	0.00E+00	1.44E+00	1.20E+01
11	0.00E+00	1.69E+00	1.30E+01
12	0.00E+00	1.96E+00	1.40E+01
13	0.00E+00	2.25E+00	1.50E+01

Table 3. Cross-sectional mechanical properties of the flexible and curved beam.

Beam Elemnt mass Density	Flap and Edge Mass Moments of Inertia per Unit Span	Flap Stiffness	Edge Stiffness	Flap Shear Stiffness	Edge Shear Stiffness	Torsional Stiffness
kg/m	kg·m	N·m²	N·m²	N·m²	N·m²	N·m²
50	50	1.00E+06	1.00E+06	5.00E+08	5.00E+08	1.00E+09

Case 3 uses the same pinned support and the same simulation scenario used in Case 2. Figure 10b shows that the initial rotational speed of 10 rpm decreases and increases with the increase and decrease of the beam inertia, respectively. The vibration behavior of the beam (shown in Figure 10b) is identical in simulations in HAWC2 and BeamDyn. The angular momentum around the rotational axis of all elements is calculated and shown in Figure 10c. It shows that the total angular momentum is conserved even when local variations of angular velocities are produced by vibrations.
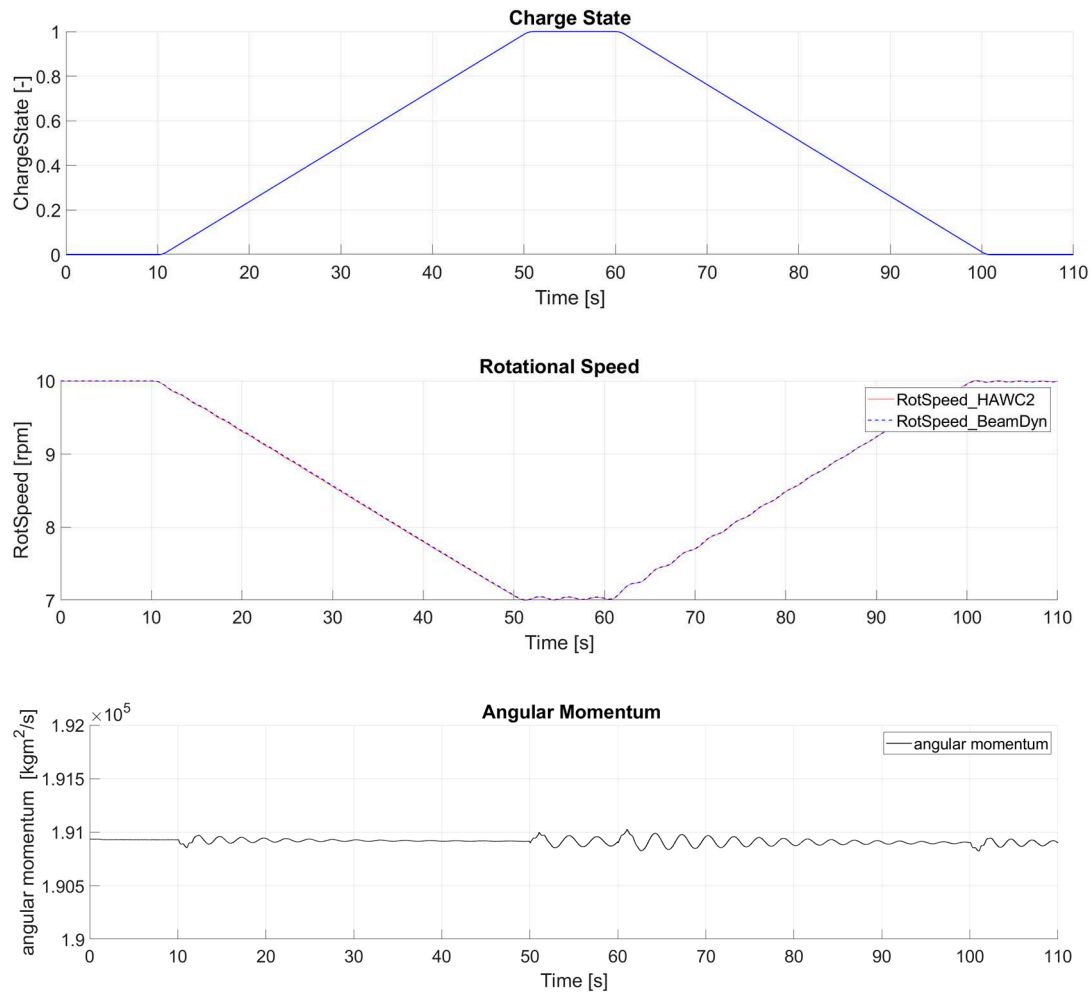
Figure 10. (a) Change in the charge state; (b) Comparison of the simulated rotational speed from HAWC2 (red) and BeamDyn (blue dashed) in a free supported, curved and flexible beam; (c) Conservation of total rotational angular momentum (black) calculated from the results of the HAWC2 simulation.

## 4. Application of the FW When the WT Performs an Emergency Braking

Numerous functionalities of the FW can be applied to deal with various grid events and to reduce the mechanical loads on the structure of WTs [6]. These functionalities are developed via the First Eigenmodes simulation model [16]. However, as discussed in the introduction, this model is not suitable for evaluating the impact of the FW on the mechanical loads of WTs. Since the validation in section 3 proved that the modified HAWC2 and BeamDyn models are able to simulate the dynamic behavior of the FW, these modified models can be used to analyze the stress reduction functionalities of the FW on WT components.

Emergency braking is one of the most drastic events that can occur to a WT. It causes significant burden on the support structures of the WT, especially on the tower bottom and on the foundation. A worst-case scenario, in which the WT has to be brought to standstill, is presented in the design load case (DLC) 2.3 in the IEC-61400-1 standards [34]. DLCs are simulation scenarios that are defined in WT guidelines, and used as a verification of WT designs. DLC 2.3 is defined as a combination of a significant wind event, i.e. extreme operation gust (EOG), with an internal or external electrical system fault, i.e. loss of electrical grid. According to the IEC-61400-1 standards, a study of several combinations of different wind speeds and times of grid loss events with respect to the EOG need to be simulated in order to determine which combination has the most critical effect on the simulated WT. Hence, a study was performed for different combination scenarios on the NREL 5 megawatt

(MW) reference WT [35]. The study showed that the combination of a rated wind speed of 11.6 m/s with a time of grid loss at the lowest wind speed in the EOG (see the event start in Figure 11a) had the greatest load effect on the WT support structure. Based on this finding, DLC 2.3 is simulated initially in the original codes of HAWC2 and OpenFAST. Figure 11a,b show that even when the wind speed, generator torque, and pitch control outputs from OpenFAST and HAWC2 are identical, the rotor speeds slightly deviate. This deviation is due to the differences in the implementation of the blade element momentum (BEM) theory in the aerodynamics models in HAWC2 [36] and OpenFAST [37]. Consequently, Figure 11c illustrates the difference in the aerodynamic torque values generated by HAWC2 and OpenFAST.

Since the aerodynamics models of HAWC2 and OpenFAST are not in the scope of the study presented in this paper, the difference in these aerodynamics models is not further investigated. However, in order to evaluate the effect of the FW on the 5 MW WT without the effect of the difference in the aerodynamics models, two comparisons are presented in Figure 12: 5 MW WT with and without FW in OpenFAST (Figure 12 right hand side), and 5 MW WT with and without FW in HAWC2 (Figure 12 left hand side).

As the generator torque disappears due to the sudden grid loss, see Figure 11a, the WT has to be brought to standstill fast to avoid excessive overspeed. This is done by quickly pitching the blade to feather position from 0° to 90°, see Figure 11b, i.e. aerodynamic emergency breaking. However, the quick pitching at high rotor speeds leads to an increase in the mechanical loads on the WT support structures. This can be seen in Figure 11d as increase in the tower base fore-aft moment.
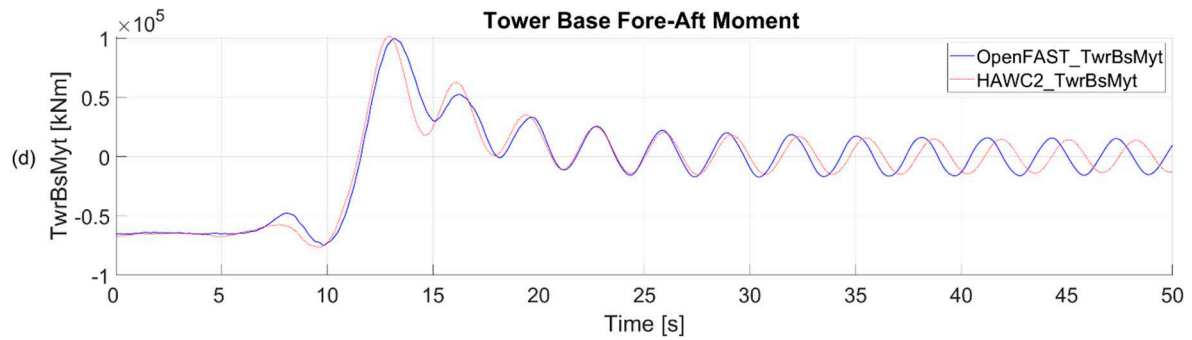
20
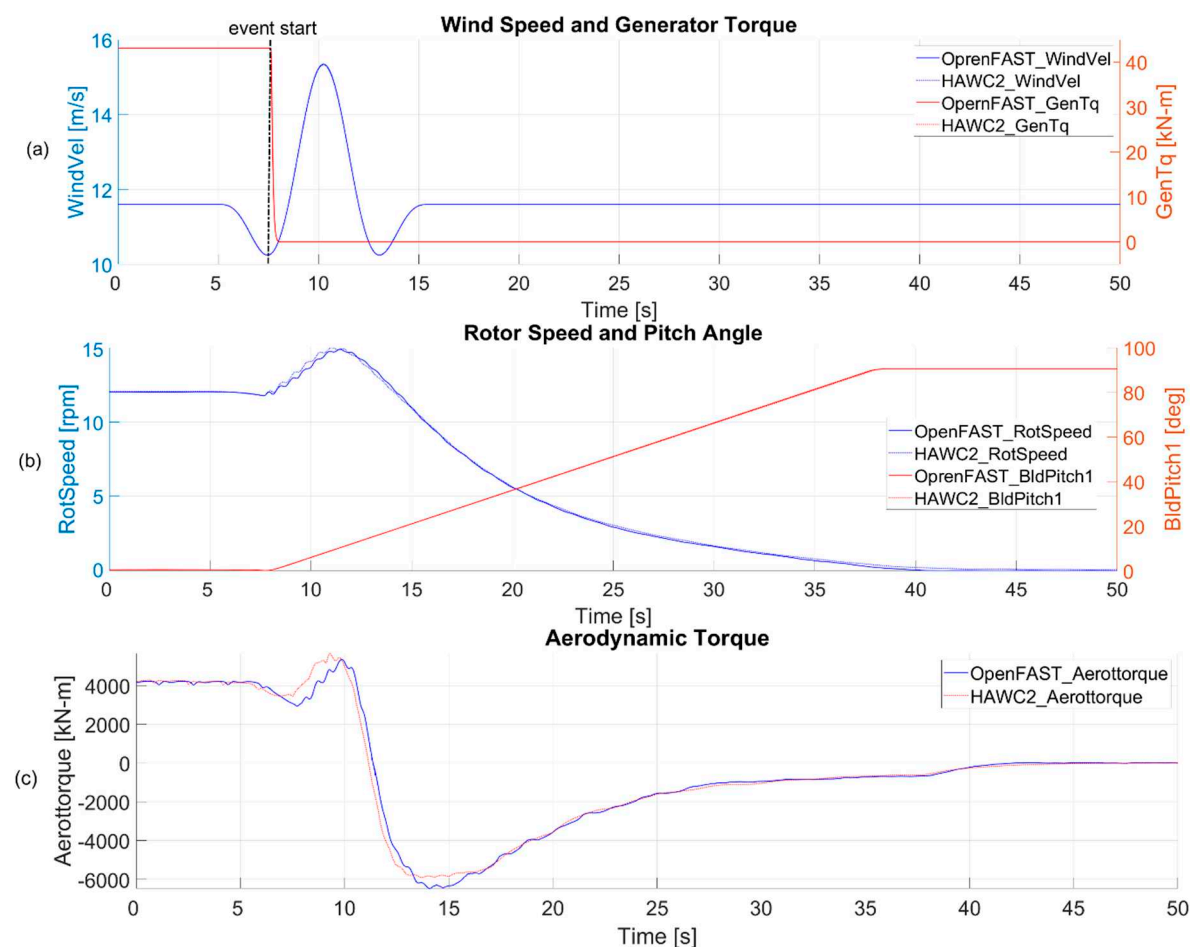
Figure 11. DLC 2.3 effect on a 5 MW refernce WT simulated with OpenFAST and HAWC2. (a) EOG with rated wind speed of 11.6 m/s and grid loss at the lowest wind speed in the gust. (b) rotor speed and pitch angle. (c) aerodynamic torque. (d) the tower base fore-aft moment.

The FW can support the aerodynamic emergency breaking in the case of DLC 2.3 by charging the FW to reach its maximum charge state in all three blades, see Figure 12a,b. Charging the FW produces two decelerating torques: a mechanical decelerating torque resulting from the Coriolis forces, see section 2.2.2, and an electrical decelerating torque at the generator by the electric pumps, see Figure 12c,d. The pumps support the charging process of the FW, and draw their power from the WT generator, even when the WT is no longer connected to the grid. In this state of operation, the generator with its frequency converter and the motors of the pumps are an electric island. Figure 12c,d illustrate the damping effect of the FW mechanical decelerating torque on the out-of-plane blade tip deflection. Figure 12a,b show that the rotor speed accelerates less when the FW is applied. The FW can decrease the tower base fore-aft moment by up to 12.5 %, see Figure 12e,f.
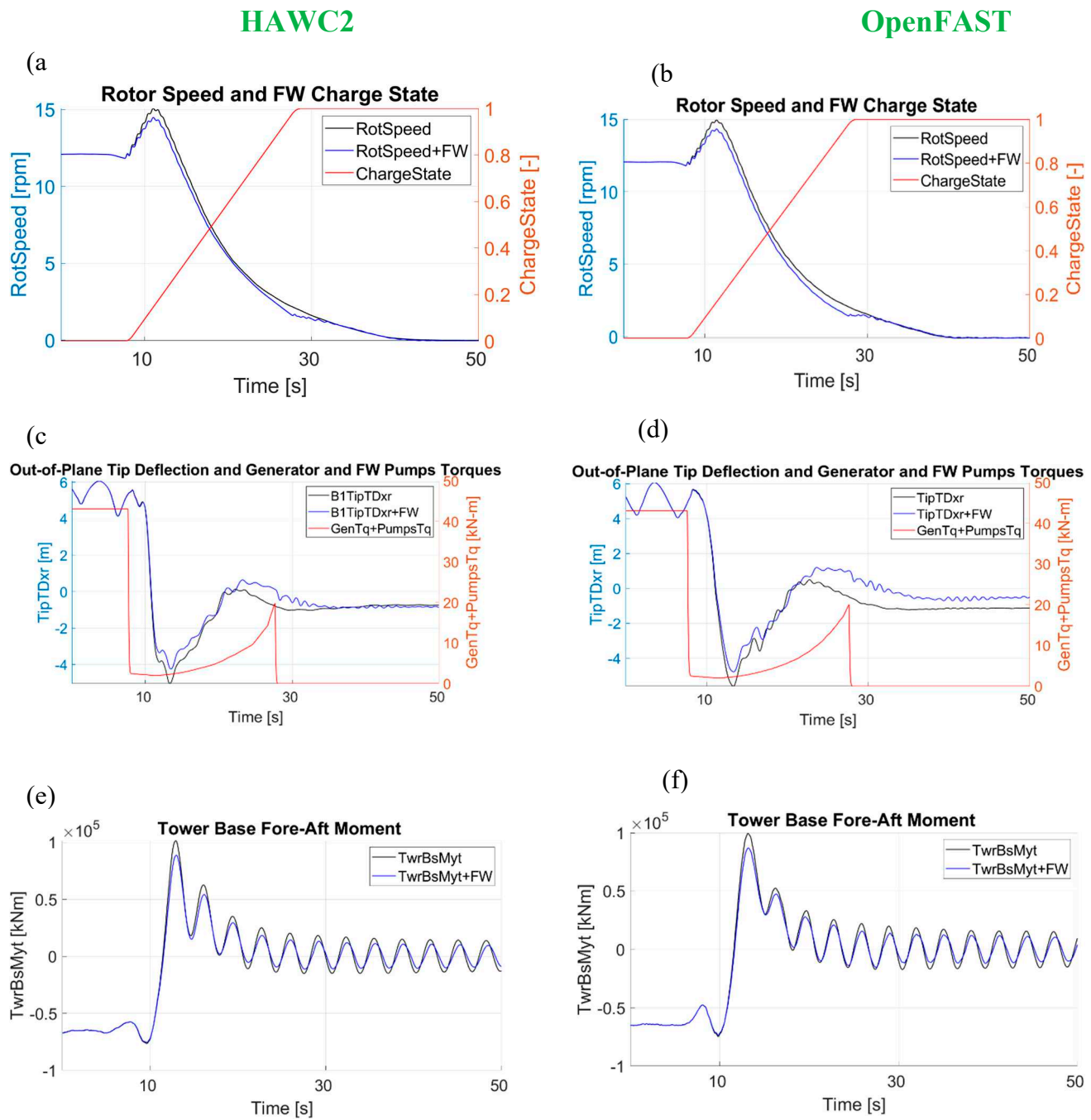
Figure 12. Comparison of the effect of DLC 2.3 on the 5 MW WT with FW (blue & red) and without FW (black) in OpenFAST and HAWC2. (a) and (b) rotational speed and charge state of the FW. (c) and (d) out-of-plane tip deflection and generator and FW pumps electrical torque. (e) and (f) tower base fore-aft bending moment.

5. Conclusions

Previous studies have investigated the effect of variable blade inertia on WTs using the First Eigenmodes simulation model [16] and the modified code of ElastoDyn [19]. The restrictions of these models and the simplified assumptions about the method used to implement variable blade inertia have necessitated an improvement to this method in more advanced structural dynamics models of

WT rotor blades. This paper presents a comparison, validation, and application of two improved methods to enable the structural dynamics models of HAWC2 and BeamDyn to simulate WTs with variable blade inertia. These two advanced models were developed to represent the nonlinear structural behavior of modern WT composite blades. Hence, they are the ideal choice for representing the extended functionality of variable blade inertia that is presented in this paper.

This paper focuses on the variation of the blade inertia from the application of FWs in WT rotors. Two methods were developed to be implemented in HAWC2 and BeamDyn. These methods were validated on the basis of three benchmarking cases of increasing complexity. For all three cases, the validation showed very good agreement between BeamDyn, HAWC2, and analytical calculations.

Simulating the application of the FW in the rotor blades of the NREL 5 MW reference WT when it is subject to DLC 2.3, shows that the FW reduces the tower base fore-aft bending moment by 12 %. This result can be yielded with both HAWC2 and OpenFAST. With the variable blade inertia, the simulated effect of the FW shows good agreement between HAWC2 and OpenFAST in the rotor blade motions, e.g. the rotor speed and the out-of-plane motion, as well as in the tower base torque.

The focus of the current research project is on the enhancement of HAWC2 and BeamDyn to simulate WTs with hydraulic-pneumatic FWs. Since, this paper shows that this goal is achieved, future work will focus on the applications of these tools to simulate different WT types with FW.

Conflicts of Interest: The author declare no conflict of interest.

References

1. Smart Blades Available online: https://www.iwes.fraunhofer.de/en/press/archive-2016/smart-blades--new-ideas-for-making-rotor-blades-more-stable-and-0.html (accessed on 30 January 2023).
2. Jauch, C.; Hippel, S. Hydraulic–Pneumatic Flywheel System in a Wind Turbine Rotor for Inertia Control. *IET Renewable Power Generation* **2016**, *10*, 33–41, doi:10.1049/iet-rpg.2015.0223.
3. Lackner, M.A.; Rotea, M.A. Passive Structural Control of Offshore Wind Turbines. *Wind Energy* **2011**, *14*, 373–388, doi:10.1002/we.426.
4. Hudecz, A.; Koss, H.; Hansen, M.O.L. Ice Accretion on Wind Turbine Blades: 15th International Workshop on Atmospheric Icing of Structures (IWAIS XV). *Proceedings of the 15th International Workshop on Atmospheric Icing of Structures (IWAIS XV)* **2013**.
5. Cacciola, S.; Agud, I.M.; Bottasso, C.L. Detection of Rotor Imbalance, Including Root Cause, Severity and Location. *J. Phys.: Conf. Ser.* **2016**, *753*, 072003, doi:10.1088/1742-6596/753/7/072003.
6. Jauch, C. Grid Services and Stress Reduction with a Flywheel in the Rotor of a Wind Turbine. *Energies* **2021**, *14*, 2556, doi:10.3390/en14092556.
7. Jauch, C. A Flywheel in a Wind Turbine Rotor for Inertia Control. *Wind Energy* **2015**, *18*, 1645–1656, doi:https://doi.org/10.1002/we.1784.
8. Hippel, S.; Jauch, C. *Hydraulic-Pneumatic Energy Storage in a Wind Turbine for Enhancing the Power System Inertia*; 2014;
9. Jauch, C. Controls of a Flywheel in a Wind Turbine Rotor. *Wind Engineering* **2016**, *40*, 173–185, doi:10.1177/0309524X16641577.
10. Alhrshy, L.; Jauch, C.; Bünning, N.; Schaffarczyk, A. Development of a Lightweight Hydraulic-Pneumatic Flywheel System for Wind Turbine Rotors. **2021**, doi:10.13140/RG.2.2.13569.89447.
11. Lackner, M.A.; Rotea, M.A. Structural Control of Floating Wind Turbines. *Mechatronics* **2011**, *21*, 704–719, doi:10.1016/j.mechatronics.2010.11.007.
12. Active Structural Control with Actuator Dynamics on a Floating Wind Turbine Available online: https://arc.aiaa.org/doi/10.2514/6.2013-455 (accessed on 15 March 2023).

13. Stewart, G.; Lackner, M. Offshore Wind Turbine Load Reduction Employing Optimal Passive Tuned Mass Damping Systems. *IEEE Transactions on Control Systems Technology* **2013**, *21*, 1090–1104, doi:10.1109/TCST.2013.2260825.

14. Stewart, G.M.; Lackner, M.A. The Effect of Actuator Dynamics on Active Structural Control of Offshore Wind Turbines. *Engineering Structures* **2011**, *33*, 1807–1816, doi:10.1016/j.engstruct.2011.02.020.

15. Stewart, G.M.; Lackner, M.A. The Impact of Passive Tuned Mass Dampers and Wind–Wave Misalignment on Offshore Wind Turbine Loads. *Engineering Structures* **2014**, *73*, 54–61, doi:10.1016/j.engstruct.2014.04.045.

16. Jauch, C. First Eigenmodes Simulation Model of a Wind Turbine - for Control Algorithm Design. **2020**, doi:10.13140/RG.2.2.17192.19204.

17. 4.2.7. ElastoDyn Users Guide and Theory Manual — OpenFAST v3.4.1 Documentation Available online: https://openfast.readthedocs.io/en/main/source/user/elastodyn/index.html#elastodyn-users-guide-and-theory-manual (accessed on 28 March 2023).

18. Jonkman, J. The New Modularization Framework for the FAST Wind Turbine CAE Tool. In Proceedings of the 51st AIAA Aerospace Sciences Meeting including the New Horizons Forum and Aerospace Exposition; American Institute of Aeronautics and Astronautics: Grapevine (Dallas/Ft. Worth Region), Texas, January 7 2013.

19. Alhrshy, L. Implementation of Variable Blade Inertia in OpenFAST to Integrate a Flywheel System in the Rotor of a Wind Turbine. *Energies* **2021**, *14*, 2783, doi:10.3390/en14102783.

20. Kane, T.R.; Levinson, D.A. *Dynamics, Theory and Applications*; McGraw Hill, 1985; ISBN 978-0-07-037846-9.

21. Larsen, T.J.; Hansen, A.M. How 2 HAWC2, the User's Manual Available online: https://tools.windenergy.dtu.dk/HAWC2/manual/How2HAWC2_12_9.pdf.

22. Wang, Q.; Sprague, M.A.; Jonkman, J.; Johnson, N.; Jonkman, B. BeamDyn: A High-Fidelity Wind Turbine Blade Solver in the FAST Modular Framework. *Wind Energy* **2017**, *20*, 1439–1462, doi:10.1002/we.2101.

23. Pavese, C.; Kim, T.; Energy, D.W. HAWC2 and BeamDyn: Comparison Between Beam Structural Models for Aero-Servo-Elastic Frameworks. 11.

24. Shabana, A.A. *Dynamics of Multibody Systems*; 1st ed.; Cambridge University Press, 2020; ISBN 978-1-108-75755-3.

25. Hansen, A.M.; Larsen, T.J. Gear Dynamics. *Research in Aeroelasticity EFP-2007-II* **2009**, 134–142.

26. Featherstone, R. Contact, Impact, and Kinematic Loops. In *Robot Dynamics Algorithms*; Featherstone, R., Ed.; The Springer International Series in Engineering and Computer Science; Springer US: Boston, MA, 1987; pp. 153–195 ISBN 978-0-387-74315-8.

27. Hodges, D.H. *Nonlinear Composite Beam Theory*; Progress in astronautics and aeronautics; American Institute of Aeronautics and Astronautics: Reston, Va., 2006; ISBN 978-1-56347-832-1.

28. Patera, A.T. A Spectral Element Method for Fluid Dynamics: Laminar Flow in a Channel Expansion. *Journal of Computational Physics* **1984**, *54*, 468–488, doi:10.1016/0021-9991(84)90128-1.

29. Bauchau, O.A.; Epple, A.; Heo, S. Interpolation of Finite Rotations in Flexible Multi-Body Dynamics Simulations. *Proceedings of the Institution of Mechanical Engineers, Part K: Journal of Multi-body Dynamics* **2008**, *222*, 353–366, doi:10.1243/14644193JMBD155.

30. Wang, Q.; Yu, W. Geometrically Nonlinear Analysis of Composite Beams Using Wiener-Milenković Parameters. *Journal of Renewable and Sustainable Energy* **2017**, *9*, 033306, doi:10.1063/1.4985091.

31. What Is an S-Function? - MATLAB & Simulink - MathWorks Deutschland Available online: https://de.mathworks.com/help/simulink/sfg/what-is-an-s-function.html (accessed on 26 June 2023).

32. Write Level-2 MATLAB S-Functions - MATLAB & Simulink - MathWorks Deutschland Available online: https://de.mathworks.com/help/simulink/sfg/writing-level-2-matlab-s-functions.html (accessed on 26 June 2023).

33. Jonkman, J.M.; Buhl, M.L.Jr. *FAST User's Guide - Updated August 2005*; 2005; p. NREL/TP-500-38230, 15020796;

34. IEC 61400-1:2019 RLV | IEC Webstore | Rural Electrification, Wind Power Available online: https://webstore.iec.ch/publication/64648 (accessed on 12 June 2023).

35. Jonkman, J.; Butterfield, S.; Musial, W.; Scott, G. Definition of a 5-MW Reference Wind Turbine for Offshore System Development. *System Development* **2009**, 75.

36. Madsen, H.A.; Larsen, T.J.; Pirrung, G.R.; Li, A.; Zahle, F. Implementation of the Blade Element Momentum Model on a Polar Grid and Its Aeroelastic Load Impact. *Wind Energy Science* **2020**, *5*, 1–27, doi:10.5194/wes-5-1-2020.
37. Jonkman, J.M.; Hayman, G.J.; Jonkman, B.J.; Damiani, R.R.; Murray, R.E. AeroDyn V15 User's Guide and Theory Manual. *Renewable Energy*.